



Cite this: *RSC Adv.*, 2022, 12, 30253

# Corn cob biochar combined with *Bacillus subtilis* to reduce Cd availability in low Cd-contaminated soil†

Yilin Yang,<sup>a</sup> Xiaojun Hu,<sup>b</sup> <sup>\*,a</sup> Huifeng Wang,<sup>\*,a</sup> Xinling Zhong,<sup>a</sup> Kaishan Chen,<sup>a</sup> Biao Huang<sup>b</sup> and Chunxiang Qian<sup>c</sup>

Soil contamination by heavy metals such as Cd can pose a risk to the environment and human health. However, Cd is difficult to immobilize at low concentration levels in soil. Individually, *Bacillus subtilis* and biochar have been shown to be inefficient at immobilizing Cd in soil. In this study, corn cob biochar was generated at different pyrolysis temperatures (300 °C–550 °C), and the Cd immobilization efficiency and performance of corn cob biochar loaded with *B. subtilis* (CB@B) and corn cob biochar alone (CB) were evaluated in solutions and in soil. The characterization (SEM and FTIR) of CB generated at different pyrolysis temperatures and CB generated at different pyrolysis temperatures in CB@B (300 °C–550 °C) indicated that a superior pore structure and abundant O-functional groups were obtained at a pyrolysis temperature of 400 °C for both CB@B and CB. The X-ray diffraction and X-ray photoelectron spectroscopy results indicate that the formation of Cd compounds was associated with the positive combined biosorption effect of the bacteria and biochar, electronic adsorption, activity of the O-functional groups (C=O, COOH, OH, and Si–O–Si), and complexation between extracellular substances and Cd<sup>2+</sup>. Adsorption experiments were conducted in a solution to assess the effects of various operating parameters such as the time, pH, and adsorbent dose. The 400 °C-CB@B and 400 °C-CB samples achieved the largest reductions in the Cd concentration at 81.21% and 5.70%, respectively. Then, CaCl<sub>2</sub> extraction experiments were conducted in soil, and using 0.25%-CB@B, a 55.21% decrease was realized in the Cd concentration after 56 days and a 16.71% increase was realized in soil pH to 8.38. No significant difference was observed in the CB-treated groups, among which 1.0%-CB achieved the largest reduction of 26.08% after 56 days and a 3.20% increase in the soil pH to 7.41. The Tessier sequential extraction method obtained similar trends. Overall, 400 °C-CB@B demonstrated outstanding immobilization efficiency and durability, indicating that it provided a safe and nutrient-rich habitat for *B. subtilis* to realize a synergistic effect for Cd immobilization.

Received 25th July 2022  
Accepted 10th October 2022

DOI: 10.1039/d2ra04643a

rsc.li/rsc-advances

## 1 Introduction

Soil pollution, particularly contamination by heavy metals such as cadmium (Cd), is deemed a serious environmental concern.<sup>1–3</sup> The Yangtze River Delta is one of the most developed areas in eastern China, and its soil has been contaminated by the occurrence of heavy metals caused by intensive anthropogenic activities.<sup>4,5</sup> Cd contamination of agricultural soil mainly results from human activities such as chemical fertilization and municipal waste extraction and incineration.<sup>6</sup> Cd easily accumulates in various plant tissues, and it can negatively affect

human health when it enters the food chain.<sup>7</sup> Excess Cd in the human body may damage the kidneys and liver, increase the risk of upper gastrointestinal cancer, and cause neurological disorders.<sup>8,9</sup>

Techniques such as chemical/biological leaching and plant extraction have been used to extract Cd from contaminated soil. Another approach is solidification/stabilization using natural or chemical/biosynthetic amendments to reduce the mobility and bioavailability of Cd in the soil.<sup>10–13</sup> Stabilization has been successfully applied to the remediation of Cd-contaminated agricultural soil because of its economic efficiency, environmental compatibility, and adaptability to the growth cycle of crops.<sup>14,15</sup> Biochar is a common organic material used for stabilization because of its low cost and applicability to energy production and climate change mitigation through carbon sequestration.<sup>16–18</sup> Corn cob biochar is obtained *via* pyrolysis, and it contains high levels of carbon and lignocellulosic biomass<sup>15</sup> with a high surface area.<sup>19,20</sup> However, unmodified biochar is generally inefficient at removing heavy metals from

<sup>a</sup>School of Chemical and Environmental Engineering, Shanghai Institute of Technology, Shanghai 201418, China. E-mail: hu-xj@sit.edu.cn; hfwang@sit.edu.cn

<sup>b</sup>Institute of Soil Science, Chinese Academy of Sciences, Nanjing, Jiangsu, 210008, China

<sup>c</sup>School of Materials Science and Engineering, Southeast University, Nanjing, Jiangsu, 211189, China

† Electronic supplementary information (ESI) available. See DOI: <https://doi.org/10.1039/d2ra04643a>


solutions. Thus, various physical modifications and chemical modifications to biochar, such as particle size modification,<sup>21</sup> acid modification, alkaline modification,<sup>22,23</sup> loading with metal oxides<sup>24</sup> or carbon materials, and combination with nanotechnology, have been investigated to increase its heavy-metal-removal efficiency. However, the above synthetic amendments often employ potentially toxic chemicals that pose a further risk to the environment and reduce their sustainability.<sup>25</sup>

In contrast, microbial amendments employ green materials and consume less energy and natural resources than the abovementioned techniques. Microbial amendments are an efficient, ecofriendly, and cost-effective method for remediating Cd-contaminated agricultural soil.<sup>26</sup> Heavy-metal-resistant bacteria such as *Bacillus megaterium* H3 and *Neorhizobium huautlense* T1-17 have been shown to significantly reduce Cd levels in the roots and grains of rice plants.<sup>10</sup> *Bacillus subtilis* (*B. subtilis*) can resist the stress from Cd adsorption, and the intracellular adsorption is relatively stable; consequently, Cd is generally not released back into the environment.<sup>27,28</sup> Moreover, *B. subtilis* produces bacteriocins that have broad spectrum antibacterial properties with significant acid, alkali, and high temperature resistances<sup>29</sup> while being harmless to humans.<sup>30,31</sup> In addition, combining biochar and microorganisms allows the former to provide essential nutrients and attachment points for the latter, which facilitates the survival and growth of exogenous bacteria when introduced to new soil<sup>32,33</sup> and reduces the nutritional deficiency of the soil.<sup>34</sup> Therefore, amendments combining biochar and bacteria have been widely used for soil remediation.

Most remediation studies have focused on soils with moderate to severe levels of heavy metal pollution.<sup>35–37</sup> Low concentration levels of soil pollution are most common,<sup>38</sup> but only few studies have focused on low Cd-contaminated soil. Moreover, low levels of Cd contamination may increase the risk of Cd accumulation in crops. Furthermore, most remediation studies on Cd-contaminated soil using bacterial agents and biochar have focused on the individual efficiency of the bacterial agents or biochar and have ignored the interaction between them. In this study, an ecofriendly and cost-effective amendment combining corn cob biochar with *B. subtilis* was applied to treat low Cd-contaminated soil. The stabilization efficiency, equilibrium, optimal dosage, and optimal amendment time were assessed. The primary objectives were to (1) prepare corn cob biochar (CB) at different pyrolysis temperatures and characterize CB loaded with *B. subtilis* (CB@B) and CB alone; (2) determine the CB and CB@B samples with the best Cd adsorption performances in a solution; and (3) explore the Cd adsorption mechanisms of the best CB and CB@B samples in soil.

## 2 Materials and methods

### 2.1 Preparation, synthesis, and characterization

Corn cobs were crushed and passed through a 100-mesh sieve. They were then pyrolyzed in a tubular furnace (Droide Instrument and Equipment Co., Ltd., Shanghai, China) under continuous N<sub>2</sub> flow at a heating rate of 5 °C min<sup>-1</sup> until the

selected pyrolysis temperature was reached (300 °C, 350 °C, 400 °C, 450 °C, 500 °C, and 550 °C), which was then maintained for 2 h. The produced CB was ground and passed through a 100-mesh sieve. The heavy metal content in the fired biochar was measured using an E-max X-ray fluorescence spectrum analyzer (XRF, XOS company, USA). The total Cd content was digested by adding HNO<sub>3</sub>, HCl, HF, and HClO<sub>4</sub> in sequential order and was then measured through inductively coupled plasma optical emission spectroscopy (ICP-OES, Optima, 2000; PerkinElmer Co., USA; Table S1†). The detection limit was 0.03 mg kg<sup>-1</sup>.<sup>39</sup>

*B. subtilis* is a urease-producing bacterial strain, and it was obtained from the China Center of Industrial Culture Collection (*B. subtilis* strain number: BNCCI 193111). Prior to the experiments, the instruments, reagents, and glassware were sterilized using a high-pressure steam sterilizer. The experimental procedures were performed on an ultraclean workbench. For bacterial cultivation, 2 g of *B. subtilis* was added to 100 mL of Luria-Bertani (LB) sterile liquid medium after autoclaving, which was then cultivated for 15 h at 30 °C. The first generation was added to 100 mL of a fresh sterile medium such that the bacterial concentration in the solution was 5%. The Erlenmeyer flask was shaken at a speed of 180 rpm at 30 °C, and the solution was cultivated for 8 h to obtain the second generation. These steps were repeated until the third generation was cultivated. The third generation of the bacillus solution was mixed with CBs prepared at different pyrolysis temperatures at a mixture-to-water ratio of 4:5 (W/V) in 250 mL Erlenmeyer flasks, which were then shaken for 2 h at 180 rpm and at 30 °C. The mixture was then filtrated and dried at 30 °C to obtain the composite amendment (CB@B) at -4 °C. CB and CB@B were characterized using a scanning electron microscope (SEM) and Fourier transform infrared spectrometer (FTIR, Nicolet IS5, USA) at a resolution of 2 cm<sup>-1</sup> in the range of 4000–400 cm<sup>-1</sup>.

### 2.2 Cd adsorption in solution

**2.2.1 Adsorption experiments in solution.** Analytical-grade Cd nitrate was used to prepare a Cd<sup>2+</sup> solution. Then, 80 mg of CB was added to the prepared Cd(NO<sub>3</sub>)<sub>2</sub> solution, which had a Cd concentration of 1.0 mg L<sup>-1</sup> to reflect the Cd concentration in soil. The solution was then shaken at 180 rpm for 24 h. The samples were tested *via* ICP-OES after being filtered through a 0.45 μm membrane filter. The above experimental procedures were repeated for CB@B. The CB@B samples were optimized for Cd adsorption performance considering the bacterial growth environment, pH conditions (3–8), CB@B dose (0–160 mg), and reaction time (1–48 h). The results (Fig. S1†) indicate that the best adsorption performance was obtained at pH 8, a CB@B dose of 80 mg, and a reaction time of 24 h. To eliminate other interfering factors, only *B. subtilis*, LB medium, 400°C-CB, and 400°C-CB@B were used to treat a solution containing 1.0 mg L<sup>-1</sup> Cd (Fig. S2†). The adsorption experiment and batch experiments began in February 2021 and ended in May 2021.

The 400°C-CB@B sample was characterized using SEM, energy dispersive spectrometry (SEM-EDS), FTIR, X-ray photoelectron spectroscopy (XPS), and X-ray diffraction (XRD, TD-



3500 Dandong Tongda Science and Technology, China) before and after being subjected to  $1.0 \text{ mg L}^{-1} \text{ Cd}$ .

**2.2.2 Models of the sorption kinetics.** Batch adsorption experiments were conducted at an initial Cd concentration of  $1.0 \text{ mg L}^{-1}$  using a  $400^\circ\text{C}$ -CB@B dose of  $80 \text{ mg}$ . The experiments lasted for 48 h according to the kinetic data. The other experimental conditions were as described in Section 2.2.1.

Three mathematical models were applied to the sorption kinetics: the intraparticle diffusion kinetic model, pseudo-first-order kinetic model, and pseudo-second-order kinetic model. These are presented below.

$$\text{Intraparticle diffusion: } q_t = C + K_i t^{0.5} \quad (1)$$

$$\text{Pseudo-first-order: } \ln(q_e - q_t) = \ln q_e - K_1 t \quad (2)$$

$$\text{Pseudo-second-order: } q_t = \frac{K_2 q_e^2 t}{1 + K_2 q_e t} \quad (3)$$

Here,  $K_i$  ( $\text{mmol g}^{-1} \text{ h}^{-1/2}$ ) is the rate constant of intraparticle diffusion and  $C$  is the intercept.  $q_e$  is the amount of  $\text{Cd}^{2+}$  adsorbed on CB@B ( $\text{mg g}^{-1}$ ) at equilibrium,  $q_t$  ( $\text{mg g}^{-1}$ ) is the  $\text{Cd}^{2+}$  concentration at time  $t$  (h), and  $T$  is  $t$  (min).  $K_1$  and  $K_2$  ( $\text{mg g}^{-1} \text{ h}^{-1}$ ) are the constants of the pseudo-first-order and pseudo-second-order reactions, respectively.

### 2.3 Cd immobilization in soil

**2.3.1 Sample collection.** Soil was collected from a Cd-contaminated paddy field ( $31^\circ 25' 54.93'' \text{ N}$ ,  $121^\circ 02' 59.19'' \text{ E}$ ) in Kunshan, Jiangsu Province, China. Kunshan is a representative area of the Yangtze River Delta in eastern China where the soil is polluted by heavy metals owing to rapid urbanization, industrialization, and agricultural intensification. Over the past 30 years, key industrial enterprises have developed in Kunshan, which has significantly increased the emission of industrial waste in the area. Although much of the total waste is removed, large quantities of waste remain in the environment, which has significantly impacted the water, soil, atmosphere, and living organisms.<sup>4</sup>

Samples were collected from the top layer (0–20 cm) of the soil, air-dried, passed through a 100-mesh sieve, and bottled for the experiments. The soil pH was measured using a pH meter (Sartorius PB-10, Beijing, China) at a solid–liquid ratio of 1 : 2.5 (W/V). The levels of heavy metals and their physicochemical properties are listed in Table S2.† The Cd concentration in the soil was  $1.4 \text{ mg kg}^{-1}$ , and the soil pH was 7.2.

**2.3.2 Soil incubation experiment.** In this experiment, 250 g of contaminated air-dried soil samples was placed in 500 mL beakers, and CB@B at dry weight concentrations of 0%, 0.25%, 0.50%, 1.00%, and 2.00% was thoroughly mixed with the soil. Each treatment was repeated thrice, and the soil was incubated at  $27^\circ\text{C}$ .<sup>40</sup> The moisture content of the soil was maintained at 70% field capacity in each beaker.<sup>7,41</sup> After 7, 14, and 56 days of incubation, the soil samples were collected, dried, and stored for further analyses after sieving with a 100-mesh sieve. The incubation periods were selected because the mature period of leafy vegetables is approximately 56 days.<sup>3</sup> The  $\text{CaCl}_2$  extraction and Tessier sequential extraction methods were then applied to

analyze the soil samples for changes in the heavy metal speciation. The  $\text{CaCl}_2$ -extractable Cd contents of the amended soil samples were extracted by  $\text{CaCl}_2$  (0.01 M) for 2 h.<sup>42</sup> The filtrates were analyzed for Cd *via* ICP-OES. The Tessier sequential extraction method<sup>43</sup> was used to investigate the speciation of Cd in the biochar-amended soil. All Cd concentrations were determined using ICP-OES. The soil incubation experiment began in July 2021 and ended in October 27, 2021.

### 2.4 Statistical analysis

XRF was only used to detect the concentrations of different heavy metals in CB and soil. One-way analysis of variance (ANOVA) with Duncan's test ( $p < 0.05$ ) was applied in SPSS 26 for Windows (SPSS Inc. IBM Corporation, USA) to determine any significant differences in the Cd recovery. The results were expressed as the mean  $\pm$  standard deviation of three independent replicates. All figures were generated using Origin (version 2018).

## 3 Results and discussion

### 3.1 Characterization of CB and CB@B

**3.1.1 Scanning electron microscopy.** The SEM results (Fig. 1) clearly show pore channels in CB that became denser with increasing temperature.<sup>44</sup> The surface area resulting from the formed pores and gaps significantly increased at temperatures above  $400^\circ\text{C}$ . At  $500^\circ\text{C}$ , CB was further pyrolyzed, which resulted in the destruction of the cellulose skeleton, decomposition of lignin, and collapse of the pore walls to form a loose pore structure. At temperatures above  $550^\circ\text{C}$ , the internal section of CB was crushed, which left only some small grooves inside the structure.

**3.1.2 Fourier transform infrared spectroscopy.** To investigate the functional groups of CB and CB@B, FTIR was conducted to detect the changes in vibrational frequencies at different pyrolysis temperatures (Fig. 2). The amplitudes were clearer for CB@B than for CB, indicating that the CB@B samples contained more functional groups than the CB samples. A vibration band at  $3426.48\text{--}3438.47 \text{ cm}^{-1}$  was attributed to hydroxyl stretching, and a C–H asymmetric vibration band at  $2922.89\text{--}2928.97 \text{ cm}^{-1}$  was attributed to fatty

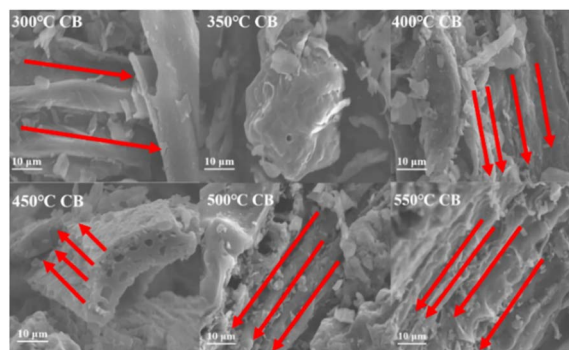


Fig. 1 SEM images of CB generated at different pyrolysis temperatures.



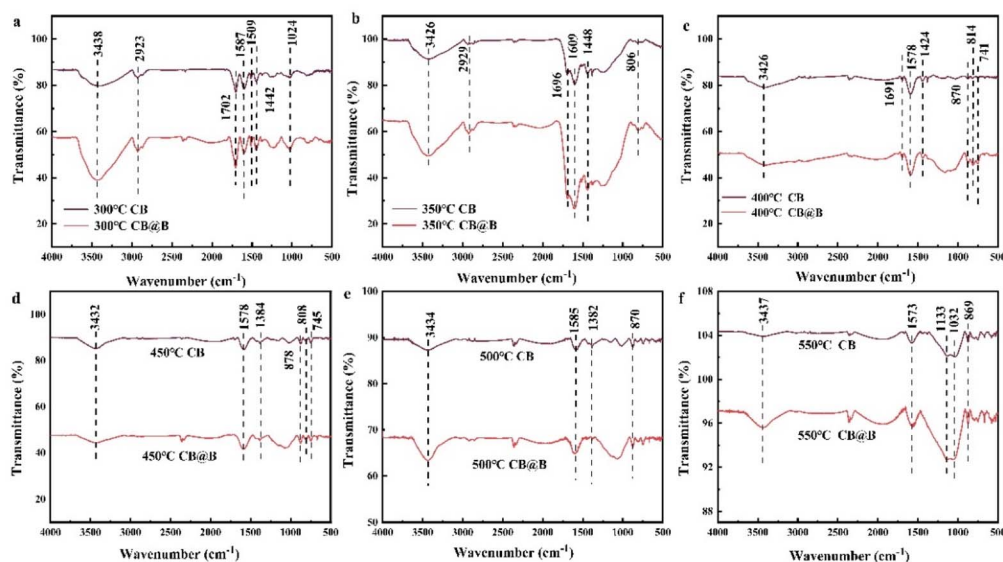


Fig. 2 FTIR images of CB and CB@B generated at different pyrolysis temperatures.

methyl groups. COOH and C–C stretching vibration peaks of benzene derivatives and a C–O stretching vibration peak of conjugated ketones and quinones were observed at 1384.53–1702.12  $\text{cm}^{-1}$ .<sup>40,45</sup> The absorption band at 741.60–878.23  $\text{cm}^{-1}$  was assigned to C–H groups.<sup>46</sup> The sorption peak near 1240  $\text{cm}^{-1}$  was attributed to a P–O bond of the phosphodiester group of nucleic acids and phospholipids.<sup>28</sup>

The number of functional groups decreased with increasing temperature. According to Zama, the loss of functional groups such as hydroxyl (O–H) and asymmetric C–H on methyl<sup>23</sup> can be attributed to the thermal decomposition of most functional groups at higher pyrolysis temperatures.<sup>47</sup> Temperatures above 500 °C can significantly increase the concentration of environmentally persistent free radicals in the feedstock, which can be potentially toxic to some soil microorganisms.<sup>48</sup> CB samples generated at 300 °C–400 °C contained more surface functional groups than the samples generated at 450 °C–550 °C, suggesting that the main mechanisms involved in the adsorption process are electrostatic interaction, ion exchange, and surface complexation.<sup>49</sup>

### 3.2 Adsorption results

**3.2.1 Adsorption effectiveness of CB and CB@B in a solution.** Fig. 3 illustrates the results of the adsorption experiments of Cd on CB and CB@B generated at different pyrolysis temperatures. Fig. S1† shows the effects of the pH, adsorbent dose, and reaction time on Cd adsorption. At a pyrolysis temperature of 400 °C, both CB and CB@B demonstrated significantly better Cd adsorption ( $p < 0.05$ ) than when generated at other pyrolysis temperatures. Moreover, CB@B exhibited a significantly higher adsorption rate than CB. The rate of Cd adsorption on CB@B increased as the pyrolysis temperature was increased from 300 °C to 400 °C and then stabilized as the temperature was further increased from 450 °C to 550 °C.

CB@B demonstrated significantly better adsorption than CB alone ( $p < 0.05$ ), indicating that *B. subtilis* played an extremely important role during Cd adsorption. Moreover, the experiment eliminating other interfering factors (Fig. S2†) showed that the Cd adsorption of CB@B was considerably higher than the adsorptions of Luria-Bertani and CB. The Cd adsorption of 400 °C-CB@B was higher than that of CB (Fig. 3) and *B. subtilis* alone (Fig. S2†) by 93.0% and 48.7%, respectively.

These results agree with those reported in other studies.<sup>34,50,51</sup> Combining bacteria and a mineral-based material decreased the Cd level and bioavailability in soil more effectively than when using either bacteria or the mineral-based material alone.<sup>37,50</sup> At a pyrolysis temperature of 400 °C, CB exhibited a clear porous structure, which provided more adsorption sites for bacteria and numerous functional groups on the surface that further facilitated the adsorption process.<sup>20,52,53</sup>

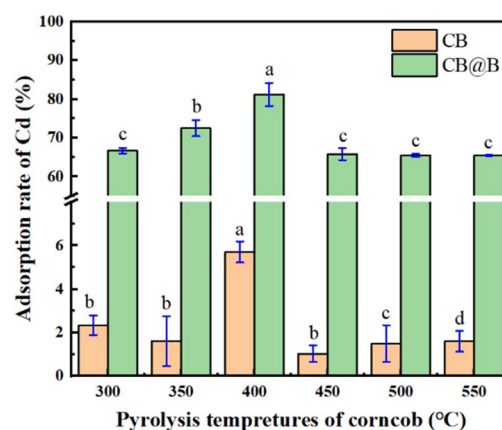


Fig. 3 Cd adsorption rate in a solution on CB and CB@B generated at different pyrolysis temperatures.





**3.2.2 Characterization of 400 °C-CB@B and 400 °C-CB@B-Cd.** Because CB and CB@B generated at 400 °C exhibited the best Cd adsorption, the pyrolysis temperature of 400 °C was used in all subsequent experiments to reduce costs and time. Fig. 4 shows the SEM-EDS results, which indicated that the living cells of *B. subtilis* became short and thick under Cd stress. The large surface area of CB facilitated the contraction of the cells under Cd stress in the solution.<sup>54</sup> Several secretions were observed between cells under Cd stress, which may bond Cd into the cellular organs and cytoplasm through chelation.<sup>28</sup> Moreover, CB may provide a habitat for colonization and protect *B. subtilis* from direct competition with other bacteria,<sup>55</sup> which would enhance the activity and functionality of the microbial community.<sup>34,56</sup> The mechanism for *B. subtilis* adsorption can be divided into two steps: (1) adsorption by active transport followed by sequestration of Cd inside the bacterial cells,<sup>2,36,37,57</sup> and (2) adsorption and chelation by the extracellular polymer substances and bacterial secretion outside the bacterial cells.<sup>37,58,59</sup> The EDS spectra indicated a Cd peak in *B. subtilis* after being subjected to 1.0 mg L<sup>-1</sup> Cd, which confirms that Cd adsorbed onto *B. subtilis*.

FTIR was conducted on CB@B before and after Cd<sup>2+</sup> adsorption (Fig. 5a). The adsorption bands around 3450 and 3440 cm<sup>-1</sup> were attributed to hydroxyl stretching vibrations.<sup>60</sup> The broad bands observed between 1620 and 1610 cm<sup>-1</sup> were assigned to the carbonyl bending vibrations.<sup>58</sup> The intense peak at 1490–1792 cm<sup>-1</sup> was attributed to the abundance of the carbonate group such as C=O.<sup>47</sup> After Cd<sup>2+</sup> adsorption on CB@B, a tiny peak was observed at 1530 cm<sup>-1</sup> that was attributed to carbonyl bending vibration. Moreover, the peak at 1610 cm<sup>-1</sup> shifted to 1620 cm<sup>-1</sup>, indicating that the carbonyl peak is closely associated with Cd immobilization.<sup>40,49</sup> At 795 cm<sup>-1</sup>, another tiny peak was observed, and the FTIR peak at 886 cm<sup>-1</sup> shifted to 891 cm<sup>-1</sup>. This new peak was related to the Si–O–Si shift, which indicates that Cd was exchanged with Si–O–Si on the surface of CB@B and formed chemical bonds. The FTIR peak at 3440 cm<sup>-1</sup> shifted to 3450 cm<sup>-1</sup>, which reflects the hydroxyl shift. These results indicate that carboxyl and phenolic hydroxyl reacted with Cd<sup>2+</sup> to form surface complexes. The reaction of these organic functional groups shifted the COOH,

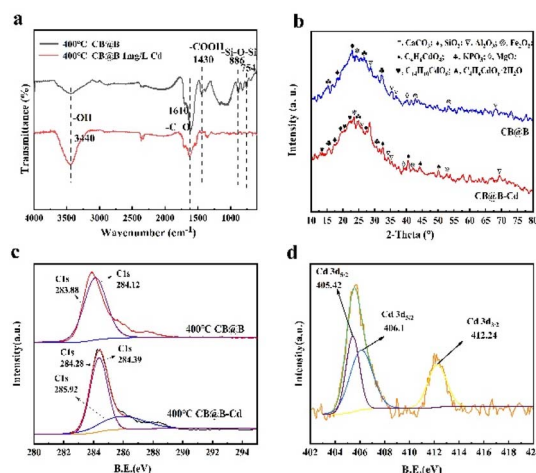


Fig. 5 (a) FTIR spectra, (b) XRD spectra, (c) C 1s XPS diagrams, and (d) Cd 3d XPS diagrams of 400 °C-CB@B before and after Cd adsorption.

OH, C=O, and Si–O–Si peaks.<sup>20,61</sup> In addition, the carboxyl functional groups of biochar may promote the complexation of heavy metals.<sup>62</sup>

The XRD spectra verified the changes in the surface functional groups (Fig. 5b). Chemical compounds such as SiO<sub>2</sub>, CaCO<sub>3</sub>, and KPO<sub>3</sub> were observed in CB@B before and after Cd adsorption. The presence of Si, K, Al, Fe, and Mg was also confirmed through SEM-EDS. The spectra clearly showed new peaks of Cd compounds formed *via* Cd adsorption on CB@B and the decrease in intensity of the SiO<sub>2</sub> peak. The adsorption process may involve precipitation<sup>63</sup> within the solution and on the surfaces. The adsorption process often proceeds synergistically with other mechanisms such as ion exchange, electrostatic interaction, and surface complexation<sup>53</sup> because of the direct interaction between chemical compounds containing carbonates (*e.g.*, SiO<sub>2</sub>) and O-functional groups (*e.g.*, O–H and COOH) on CB@B and Cd.<sup>61</sup> These chemical compounds are highly effective in immobilizing heavy metals in contaminated soil.<sup>42</sup>

Before Cd adsorption, a sharp peak was observed at 283.00 eV in the C 1s narrow region spectrum (Fig. 5c), which was assigned to the carbon in aliphatic or aromatic C–H and C–C or to C=C bonds.<sup>20,23</sup> A characteristic peak was observed at 287.00 eV, which was assigned to hydroxyl carbon. After Cd adsorption, the peaks of the aliphatic carbon and hydroxyl group shifted to 284.439 and 288.231 eV, respectively, which indicated that CB@B contained aliphatic carbon and hydroxyl radicals that participated in the reaction.<sup>23</sup> This result was also confirmed by the FITR results. O-containing functional groups, especially carboxyl and hydroxyl, play an important role in the stable binding of Cd<sup>2+</sup> with biochar by complexation.<sup>52</sup> The Cd signal was not detected in CB@B before being treated with 1.0 mg L<sup>-1</sup> Cd. The presence of Cd in CB@B was detected after the treatment with Cd (Fig. 5d), which confirms the Cd adsorption and loading onto CB@B. The high-resolution XPS spectra for 3d-distributed Cd at 405.42 and 406.16 eV can be attributed to the 3d<sub>5/2</sub> track of Cd. The two characteristic peaks

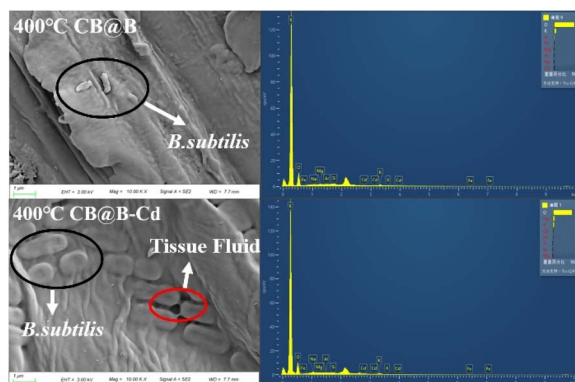


Fig. 4 SEM-EDS results of 400 °C-CB@B before and after Cd adsorption.



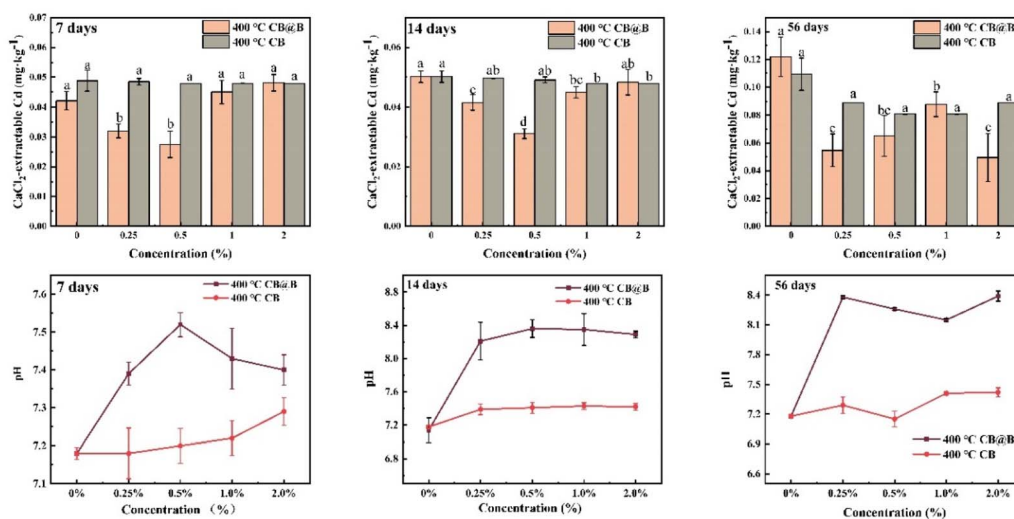


Fig. 6 Changes in the  $\text{CaCl}_2$ -extractable Cd and soil pH after treatment using  $400\text{ }^\circ\text{C}$ -CB and  $400\text{ }^\circ\text{C}$ -CB@B.

observed at 412.02 and 412.664 eV can be attributed to the  $3d_{3/2}$  track. These results indicate that Cd on CB@B was mainly in the form of  $\text{Cd}^{2+}$ .

The above results indicate that multiple mechanisms were involved in the  $\text{Cd}^{2+}$  adsorption on CB@B, including electrostatic interaction, ion exchange, complexation, chelation, and precipitation.<sup>34,64,65</sup> The adsorption mechanism of *B. subtilis* involves two steps: (1) bioaccumulation by active transport of Cd into the cell combined with the activity of extracellular substances to sequester Cd inside the bacterial cell;<sup>2,36,37,57</sup> and (2) adsorption and chelation by extracellular polymer substances combined with bacterial secretion outside the bacterial cell.<sup>37,58,59</sup>

**3.2.3 Sorption kinetics.** The three mathematical models described in Section 2.2.2 were fitted to the experimental data. The pseudo-first-order model ( $R^2 = 0.995$ ) and pseudo-second-order kinetic model ( $R^2 = 0.986$ ) fitted well to the Cd adsorption process of CB@B (Fig. S3 and Table S3†). However, the pseudo-first-order model demonstrated a better fit. The initial Cd concentration was  $1.0\text{ mg L}^{-1}$ , and the experiment ended after 48 h. The  $\text{Cd}^{2+}$  adsorption capacity of CB@B rapidly

increased at first and reached equilibrium after 24 h. After attaining equilibrium, the  $\text{Cd}^{2+}$  adsorption capacity was  $0.1205\text{ mg g}^{-1}$ . In the pseudo-first-order model, there was a period where the  $\text{Cd}^{2+}$  sorption rapidly increased with time. During this process,  $\text{Cd}^{2+}$  ions were adsorbed on the outer surface of CB and the cell walls by electrostatic adsorption and complexation of various polar functional groups.<sup>58,66</sup> CB@B reached adsorption equilibrium after 24 h of contact because of the accumulation of microorganisms accompanied by energy expenditure.<sup>27</sup> The presence of the functional groups and CB@B (e.g., COOH and OH) resulted in different adsorption mechanisms including electrostatic interaction, ion exchange, complexation, chelation, and precipitation.<sup>67</sup> The representative formulas of the adsorption reactions are given below.

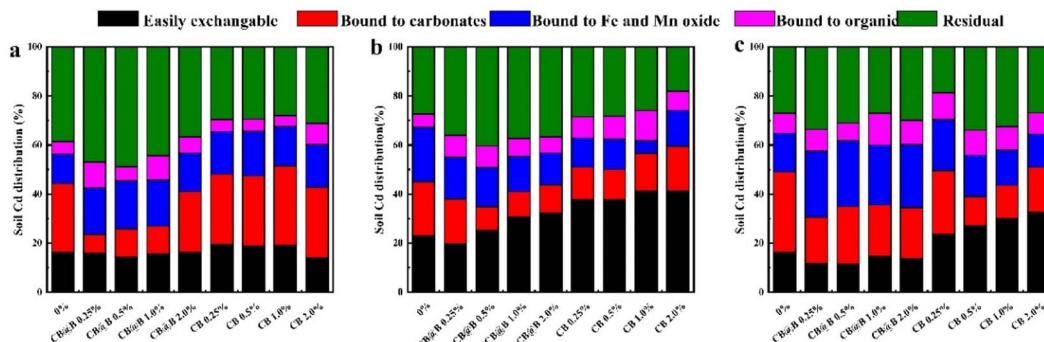
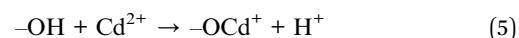
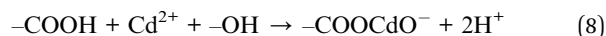
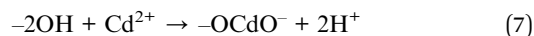


Fig. 7 Speciation of Cd in soil amended with different doses of  $400\text{ }^\circ\text{C}$ -CB and  $400\text{ }^\circ\text{C}$ -CB@B after incubation for (a) 7 days, (b) 14 days, and (c) 56 days.





Not all of the fitting lines of the intraparticle diffusion kinetic model passed through the origin of the coordinates, indicating that intraparticle diffusion was not the only rate-limiting factor.

### 3.3 Soil incubation effect of 400 °C-CB and CB@B

**3.3.1 Levels of  $\text{CaCl}_2$ -extractable Cd and pH.** Fig. 6 shows the Cd immobilization capacities of CB and CB@B. After 56 days, both CB@B concentrations (2% and 0.25%) significantly decreased the amount of  $\text{CaCl}_2$ -extractable Cd. After 7 and 14 days, 0.5% CB@B exhibited the maximum reduction of  $\text{CaCl}_2$ -extractable Cd at 38.02% and 34.72%, respectively. CB@B significantly decreased the  $\text{CaCl}_2$ -extractable Cd compared with CB and the control ( $p < 0.05$ ). A similar trend was obtained for the soil pH. The two amended soil samples always had a higher pH than the control. Increasing the soil pH can increase the number of adsorption sites with negative charges on the soil organic-inorganic colloids and clay particles,<sup>68</sup> which increases heavy metal precipitation in the form of oxides, hydroxides, carbonates, and phosphates.<sup>42</sup>

**3.3.2 Distribution of Cd fractions.** Fig. 7 indicates that the residual Cd in the untreated soil decreased with increasing incubation time, which suggests an increase in the risk of Cd entering the ecological environment. The CB@B-treated soil showed a reduction in exchangeable Cd. Compared with the control, the maximum Cd reduction after 7 days was 56.37% in the 0.25%-CB@B-amended soil, and the maximum Cd reduction after 14 days was 69.45% in the 0.5%-CB@B-amended soil. Thus, CB@B enhanced Cd immobilization by changing the exchangeable Cd fraction to carbonate-bound, oxide-bound, and organic matter-bound forms with some residual Cd. In addition, CB@B was more effective than CB. When treated with additional CB, the exchangeable Cd and carbonate Cd in the soil increased after 7 and 14 days, which may be attributed to the breakdown of organic carbon in CB, especially the aromatic moieties, into low molecular-weight organic acids.<sup>20</sup> The Tessier sequential extraction results agreed with the  $\text{CaCl}_2$  extraction results.

## 4 Conclusions

The experimental results showed that CB@B provided a habitat for exogenous bacteria, improved Cd immobilization, and reduced Cd bioavailability compared with CB alone, indicating that it is an attractive option for mitigating the risks posed by low Cd-contaminated soil. SEM results indicate that the pyrolysis temperature affects the porosity and number of functional groups on the CB surface. Under optimal conditions, CB@B exhibited the best Cd immobilization performance at a pyrolysis temperature of 400 °C and significantly decreased the Cd content in the solution by 81.21%. The characterization results for 400 °C-CB@B and 400 °C-CB indicate the presence of functional groups (e.g., C=O, COOH, and OH), compounds

(e.g.,  $\text{SiO}_2$ ,  $\text{CaCO}_3$ , and  $\text{KPO}_3$ ), and Si–O–Si on the surface of 400 °C-CB@B. The adsorption mechanism combined activity by extracellular substances and activity by O-functional groups, which promoted Cd complexation in the solution. *B. subtilis* was shown to play an important part in Cd adsorption. In experiments on low Cd-contaminated agricultural soil, 400 °C-CB@B significantly and rapidly decreased the available Cd by 55.21%, which was significantly better compared with other treatments at 7 and 14 days. The Cd immobilization in soil by 400 °C-CB@B involved physical adsorption, electrostatic interaction, and ion exchange. In conclusion, 400 °C-CB@B is an environmentally friendly, economic, and effective amendment for low Cd-contaminated soil that is easily applied by farmers whose lands are affected by heavy metal pollution. Further research is needed on the bacterial load. This study thus provides a theoretical and practical foundation for the management of low Cd-contaminated agricultural soil.

## Author contributions

Yilin Yang: formal analysis, investigation, visualization, writing—original draft; Xiaojun Hu: conceptualization, funding acquisition, supervision; Huifeng Wang: methodology, formal analysis, investigation, writing—review and editing; Xinling Zhong: formal analysis, validation; Kaishan Chen: formal analysis, investigation; Biao Huang: resources; Chunxiang Qian: resources. All authors read and approved the final manuscript.

## Conflicts of interest

There are no conflicts to declare.

## Acknowledgements

This work was supported by “Shuguang Scholar Program” (17SG52) by Shanghai Education Development Foundation, Shanghai Municipal Education Commission and Liaoning Provincial Natural Science Fund Project (2019-ZD-0550), Scientific Research Foundation of Shanghai Institute of Technology (YJ2021-26).

## Notes and references

- 1 D. Kulikowska, Z. M. Gusiatin, K. Bulkowska and B. Klik, *J. Hazard. Mater.*, 2015, **300**, 882–891.
- 2 L. Liu, J. Li, F. Yue, X. Yan, F. Wang, S. Bloszies and Y. Wang, *Chemosphere*, 2018, **194**, 495–503.
- 3 H. Wang, W. Hu, Q. Wua, B. Huang, L. Zong, A. Wang and G. S. Matthew, *J. Cleaner Prod.*, 2021, **311**, 127673.
- 4 X. L. Zhong, S. L. Zhou, Q. Zhu and Q. G. Zhao, *J. Hazard. Mater.*, 2011, **198**, 13–21.
- 5 X. Zhang, D. Chen, T. Zhong, X. Zhang, M. Cheng and X. Li, *Environ. Sci. Pollut. Res.*, 2015, **22**, 4932–4941.
- 6 X. Tang, Q. Li, M. Wu, L. Lin and M. Scholz, *J. Environ. Manage.*, 2016, **181**, 646–662.





- 7 A. Hussain, S. Ali, M. Rizwan, M. Z. U. Rehman, M. F. Qayyum, H. Wang and J. Rinklebe, *Ecotoxicol. Environ. Saf.*, 2019, **173**, 156–164.
- 8 Y. Hu, H. Cheng and S. Tao, *Environ. Int.*, 2016, **92–93**, 515–532.
- 9 H. Chen, Y. Teng, S. Lu, Y. Wang and J. Wang, *Sci. Total Environ.*, 2015, **512–513**, 143–153.
- 10 Y. Li, H. D. Pang, L. Y. He, Q. Wang and X. F. Sheng, *Ecotoxicol. Environ. Saf.*, 2017, **138**, 56–63.
- 11 C. Tu, F. Guan, Y. Sun, P. Guo, Y. Liu, L. Li, K. G. Scheckel and Y. Luo, *Geoderma*, 2018, **332**, 190–197.
- 12 M. Hong, L. Zhang, Z. Tan and Q. Huang, *Environ. Sci. Pollut. Res.*, 2019, **26**, 19738–19748.
- 13 Q. Chen, J. Dong, Q. Yi, X. Liu, J. Zhang and Z. Zeng, *ACS Sustainable Chem. Eng.*, 2019, **7**, 9928–9936.
- 14 R. Wang, S. Wei, P. Jia, T. Liu, D. Hou, R. Xie, Z. Lin, J. Ge, Y. Qiao, X. Chang, L. Lu and S. Tian, *Sci. Total Environ.*, 2019, **676**, 627–638.
- 15 P. Gu, Y. Zhang, H. Xie, J. Wei, X. Zhang, X. Huang, J. Wang and X. Lou, *Ecotoxicol. Environ. Saf.*, 2020, **205**, 111144.
- 16 B. Zhao, R. Xu, F. Ma, Y. Li and L. Wang, *J. Environ. Manage.*, 2016, **184**, 569–574.
- 17 P. Wang, X. Liu, B. Yu, X. Wu, J. Xu, F. Dong and Y. Zheng, *Sci. Total Environ.*, 2020, **702**, 134767.
- 18 H. Zhang, R. Xiao, R. Li, A. Ali, A. Chen and Z. Zhang, *Chemosphere*, 2020, **261**, 127694.
- 19 P. Kaur, P. Kaur and K. Kaur, *J. Cleaner Prod.*, 2020, 244.
- 20 F. Jing, Y. Liu and J. Chen, *Environ. Pollut.*, 2021, **291**, 118243.
- 21 A. H. Fahmi, A. W. Samsuri, H. Jol and D. Singh, *RSC Adv.*, 2018, **8**, 38270–38280.
- 22 A. U. Rajapaksha, S. S. Chen, D. C. Tsang, M. Zhang, M. Vithanage, S. Mandal, B. Gao, N. S. Bolan and Y. S. Ok, *Chemosphere*, 2016, **148**, 276–291.
- 23 H. Chen, X. Yang, Y. Liu, X. Lin, J. Wang, Z. Zhang, N. Li, Y. Li and Y. Zhang, *Waste Manage.*, 2021, **130**, 82–92.
- 24 L. Wu, C. Wei, S. Zhang, Y. Wang, Y. Kuzyakov and X. Ding, *J. Cleaner Prod.*, 2019, **235**, 901–909.
- 25 P. Zhang, D. O'Connor, Y. Wang, L. Jiang, T. Xia, L. Wang, D. C. W. Tsang, Y. S. Ok and D. Hou, *J. Hazard. Mater.*, 2020, **384**, 121286.
- 26 C.-q. Su, L.-q. Li, Z.-h. Yang, L.-y. Chai, Q. Liao, Y. Shi and J.-w. Li, *Trans. Nonferrous Met. Soc. China*, 2019, **29**, 1304–1311.
- 27 H. Huang, Q. Jia, W. Jing, H. U. Dahms and L. Wang, *Chemosphere*, 2020, **251**, 126428.
- 28 Y. Xie, N. He, M. Wei, T. Wen, X. Wang, H. Liu, S. Zhong and H. Xu, *J. Cleaner Prod.*, 2021, 312.
- 29 Y.-Z. Xiang, X.-Y. Li, H.-L. Zheng, J.-Y. Chen, L.-B. Lin and Q.-L. Zhang, *Lwt*, 2021, 146.
- 30 M. Z. Mohsin, R. Omer, J. Huang, A. Mohsin, M. Guo, J. Qian and Y. Zhuang, *Synth. Syst. Biotechnol.*, 2021, **6**, 180–191.
- 31 S. Agrawal, U. K. Jana and N. Kango, *Int. J. Biol. Macromol.*, 2021, **192**, 28–37.
- 32 T. Yu, L. Wang, F. Ma, Y. Wang and S. Bai, *J. Hazard. Mater.*, 2020, **384**, 121326.
- 33 C. Wang, Y. Huang, X. Yang, W. Xue, X. Zhang, Y. Zhang, J. Pang, Y. Liu and Z. Liu, *Chemosphere*, 2020, **252**, 126603.
- 34 X. Qi, J. Gou, X. Chen, S. Xiao, I. Ali, R. Shang, D. Wang, Y. Wu, M. Han and X. Luo, *J. Hazard. Mater.*, 2021, **401**, 123823.
- 35 A. H. Lahori, Z. Zhang, Z. Guo, R. Li, A. Mahar, M. K. Awasthi, P. Wang, F. Shen, F. Kumbhar, T. A. Sial, J. Zhao and D. Guo, *Ecotoxicol. Environ. Saf.*, 2017, **145**, 528–538.
- 36 W. Pan, Q. Lu, Q. R. Xu, R. R. Zhang, H. Y. Li, Y. H. Yang, H. J. Liu and S. T. Du, *Ecotoxicol. Environ. Saf.*, 2019, **177**, 100–107.
- 37 G. Andrey, V. Rajput, M. Tatiana, M. Saglara, S. Svetlana, K. Igor, T. V. Grigoryeva, C. Vasily, A. Iraida, Z. Vladislav, F. Elena and M. Hasmik, *Appl. Geochem.*, 2019, **104**, 93–101.
- 38 MEE, 2014.
- 39 H. Wang, Q. Wu, W. Hu, B. Huang, L. Dong and G. Liu, *Environ. Pollut.*, 2018, **243**, 1047–1056.
- 40 Y. Hamid, L. Tang, B. Hussain, M. Usman, H. K. Gurajala, M. S. Rashid, Z. He and X. Yang, *Environ. Pollut.*, 2020, **257**, 113609.
- 41 T. Ma, L. Zhou, L. Chen, Z. Li, L. Wu, P. Christie and Y. Luo, *J. Agric. Food Chem.*, 2016, **64**, 8045–8053.
- 42 S. Bashir, Q. Hussain, M. Shaaban and H. Hu, *Chemosphere*, 2018, **211**, 632–639.
- 43 Y. Yong, Y. Xu, Q. Huang, Y. Sun, L. Wang, X. Liang, X. Qin and L. Zhao, *Sci. Total Environ.*, 2022, **813**, 152636.
- 44 H. S. Kambo and A. Dutta, *Renewable Sustainable Energy Rev.*, 2015, **45**, 359–378.
- 45 H. Lyu, S. Xia, J. Tang, Y. Zhang, B. Gao and B. Shen, *J. Hazard. Mater.*, 2020, **384**, 121357.
- 46 R. Gao, Q. Fu, H. Hu, Q. Wang, Y. Liu and J. Zhu, *J. Hazard. Mater.*, 2019, **371**, 191–197.
- 47 E. F. Zama, G. Li, Y. T. Tang, B. J. Reid, N. M. Ngwabie and G. X. Sun, *Environ. Pollut.*, 2022, **292**, 118241.
- 48 E. S. Odinga, M. G. Waigi, F. O. Gudda, J. Wang, B. Yang, X. Hu, S. Li and Y. Gao, *Environ. Int.*, 2020, **134**, 105172.
- 49 D. Chen, X. Wang, X. Wang, K. Feng, J. Su and J. Dong, *Sci. Total Environ.*, 2020, **714**, 136550.
- 50 Q. Li, P. Zhang, H. Zhou, P. Q. Peng, K. Zhang, J. X. Mei, J. Li and B. H. Liao, *Ecotoxicol. Environ. Saf.*, 2020, **195**, 110492.
- 51 Y. Zhu, M. Zhong, W. Li, Y. Qiu, H. Wang and X. Lv, *Ecotoxicol. Environ. Saf.*, 2022, 232.
- 52 H. Li, X. Ye, Z. Geng, H. Zhou, X. Guo, Y. Zhang, H. Zhao and G. Wang, *J. Hazard. Mater.*, 2016, **304**, 40–48.
- 53 T. Yang, Y. Xu, Q. Huang, Y. Sun, X. Liang, L. Wang, X. Qin and L. Zhao, *Bioresour. Technol.*, 2021, **333**, 125078.
- 54 H. Han, H. Cai, X. Wang, X. Hu, Z. Chen and L. Yao, *Ecotoxicol. Environ. Saf.*, 2020, **195**, 110375.
- 55 Y. Liu, B. Tie, O. Peng, H. Luo, D. Li, S. Liu, M. Lei, X. Wei, X. Liu and H. Du, *Chemosphere*, 2020, **247**, 125850.
- 56 M. Ahmad, A. U. Rajapaksha, J. E. Lim, M. Zhang, N. Bolan, D. Mohan, M. Vithanage, S. S. Lee and Y. S. Ok, *Chemosphere*, 2014, **99**, 19–33.
- 57 H. Li, X. Li, L. Xiang, H. M. Zhao, Y. W. Li, Q. Y. Cai, L. Zhu, C. H. Mo and M. H. Wong, *Sci. Total Environ.*, 2018, **613–614**, 447–455.





- 58 T. Wang, H. Sun, X. Ren, B. Li and H. Mao, *Ecotoxicol. Environ. Saf.*, 2018, **148**, 285–292.
- 59 H. Ma, M. Wei, Z. Wang, S. Hou, X. Li and H. Xu, *J. Hazard. Mater.*, 2020, **388**, 122065.
- 60 H. P. Chen, P. Wang, J. D. Chang, P. M. Kopittke and F. J. Zhao, *Chemosphere*, 2021, **267**, 128893.
- 61 Y.-h. Fei, Z. Zhang, Z. Ye, Q. Wu, Y.-t. Tang and T. Xiao, *J. Environ. Sci.*, 2022, **113**, 64–71.
- 62 R. Gao, H. Hu, Q. Fu, Z. Li, Z. Xing, U. Ali, J. Zhu and Y. Liu, *Sci. Total Environ.*, 2020, **730**, 139119.
- 63 A. A. Houssou, P. Jeyakumar, N. K. Niazi, L. Van Zwieten, X. Li, L. Huang, L. Wei, X. Zheng, Q. Huang, Y. Huang, X. Huang, H. Wang, Z. Liu and Z. Huang, *Biochar*, 2022, 4.
- 64 R. Xiao, P. Wang, S. Mi, A. Ali, X. Liu, Y. Li, W. Guan, R. Li and Z. Zhang, *Ecotoxicol. Environ. Saf.*, 2019, **181**, 155–163.
- 65 Z. Xu, X. Xu, D. C. W. Tsang and X. Cao, *Environ. Pollut.*, 2018, **242**, 1362–1370.
- 66 Y. Yang, Y. Ge, P. Tu, H. Zeng, X. Zhou, D. Zou, K. Wang and Q. Zeng, *J. Hazard. Mater.*, 2019, **363**, 385–393.
- 67 L. Hua, T. Cheng, Z. Liang and T. Wei, *Biochar*, 2022, 4.
- 68 N. Sornhiran, S. Aramrak, N. Prakongkep and W. Wisawapipat, *Biochar*, 2022, 4.

